Notice of Violation of IEEE Publication Principles

"A Gravitational Search based Fuzzy Approach for Edge Detection in Colour And Grayscale Images"
by Swagatam Das, Satrajit Mukherjee, Bodhisattwa Prasad Majumder and Aritran Piplai
Submitted to IEEE Transactions on Fuzzy System

After careful and considered review of the content and authorship of this paper by a duly constituted expert committee, this paper has been found to be in violation of IEEE's Publication Principles.

This paper duplicates significant amounts of content from the original paper cited below. The original text was copied without attribution (including appropriate references to the original author(s) and/or paper title) and without permission.

Due to the nature of this violation, reasonable effort should be made to remove all past references to this paper, and future references should be made to the following article:

"An Optimal Fuzzy System for Edge Detection in Color Images using Bacterial Foraging Algorithm,"
by Om Verma
Submitted to IEEE Transactions on Evolutionary Computation, 12 April 2012

This article has been accepted for publication in a future issue of this journal, but has not been fully edited. Content may change prior to final publication. Citation information: DOI 10.1109/TFUZZ.2013.2286418, IEEE Transactions on Fuzzy Systems

A Gravitational Search based Fuzzy Approach for Edge Detection in Colour And Grayscale Images

Swagatam Das[1], *Senior Member, IEEE*, Satrajit Mukherjee[2], Bodhisattwa Prasad Majumder[2], and Aritran Piplai[3]

[1]Electronics and Communication Sciences Unit, Indian Statistical Institute, Kolkata – 700 108, India.
[1]Dept. of Electronics and Telecommunication Engg., Jadavpur University, Kolkata 700 032, India.
[2]Dept. of Computer Science and Engg., Jadavpur University, Kolkata 700 032, India.

E-mails: swagatam.das@isical.ac.in, satra0293@gmail.com, mbodhisattwa@gmail.com, mpiplai@yahoo.com

***Abstract*—This article presents an optimal edge detection scheme based on the concepts of fuzzy Smallest Univalue Assimilating Nucleus (SUSAN) and the Gravitational Search Algorithm (GSA). Initially, the Univalue Assimilating Nucleus (USAN) area is calculated from the gray levels of every neighborhood pixel of a pixel of interest in the test image. In accordance with the SUSAN principle, the neighborhood is chosen as a circular mask and applied separately on the individual RGB components of the image in case the image is a color image. The USAN area edge map of each component is fuzzified using a Gaussian membership function (used for detecting strong edges) and a bell-shaped function (used for detecting weak edges). Then the entropy and edge sharpness factors are calculated from these fuzzy measures and optimized using GSA by evolving the fuzzifier and the parameters controlling the shape and range of the bell-shaped curve. Adaptive thresholding converts the fuzzy domain edge map to a spatial domain edge map. Finally, the individual RGB edge maps are concatenated to obtain the final image edge map. Qualitative and quantitative comparisons have been rendered with respect to a few promising edge detectors (both traditional as well as state-of-the-art) and also optimal fuzzy edge detectors based on metaheuristic algorithms like Differential Evolution (DE) and Particle Swarm Optimizer (PSO). Extensive comparisons based on several quantitative measures strongly reflect merits of the proposed method.**

***Keywords* –** gravitational search algorithm; edge detection; USAN area; SUSAN area; fuzzifier; fuzzy entropy.

I. Introduction

Edges of an image are mainly boundaries between two regions which have great difference in their respective pixel intensities. Applications of edge detection have been greatly on the rise over the years and thus, edge detection has become a very important image processing task. Edges help to demarcate an image into objects and background. This particular functionality of edges makes the process of edge detection applicable to various fields like raw image size compression, image segmentation, contour feature extraction, thereby facilitating high-level image processing tasks.

The separation of an image into object and background pixels, by tracing the edges separating them, serves as an important step in image interpretation and analysis. Edge detectors can be broadly classified into directional [1-3] and non-directional ones [4, 5]. Directional methods generally use two masks and convolutions whereas usage of only a single mask and convolution are found in non-directional methods. However, they are subject to noise due to the gradient nature of the operators. The Canny edge detection [4, 5] algorithm works by computing the gradients at each pixel in a smoothed or de-noised image and then carrying out a search to determine if the gradient magnitude assumes local maxima in the gradient direction. Though the Canny edge detector can detect the maximum number of edges in an image, it distorts the shape of the image and leads to the formation of double edges. Roberts and Sobel edge detectors perform 2-D spatial gradient measurement on an image and highlight regions of high spatial frequency, which often correspond to edges. Zero-crossing based edge detectors like the Laplacian of the Gaussian (LoG), work by convolving the image by a Gaussian kernel and then computing second-order derivative expressions like the Laplacian to detect the edges. Non-gradient edge detectors like the SUSAN [6] detect edges in the image by associating small area of neighbourhood pixels of similar intensity to each centre pixel. However, both the LoG and the SUSAN are unable to detect weak edges and the edge connectivity is poor in case of the latter. Despite this, the value of Shannon's Entropy [7] as computed experimentally for SUSAN comes out to be high due to the presence of noise. Fuzzy measures help to extract incomplete information and thus, detect weak edges [8]. In [9] Bezdek *et al*. considered edge detection as a combination of four steps: conditioning, feature extraction, blending, and scaling. The authors explored the role of geometry in determining good features for edge detection and in setting parameters for functions to blend the features. Boskovitz and Guterman [10] presented a multilayer perceptron like network that performs image segmentation by adaptive thresholding of

This article has been accepted for publication in a future issue of this journal, but has not been fully edited. Content may change prior to final publication. Citation information: DOI 10.1109/TFUZZ.2013.2286418, IEEE Transactions on Fuzzy Systems

the input image based on the labels automatically pre-selected by a fuzzy clustering algorithm. Some fuzzy rule-based approaches to edge detection and image binarization can also be found in works like [11, 12]. Recently Barrenechea *et al*. [13] proposed a new method for constructing interval-valued fuzzy relations from fuzzy images, based on the concepts of the triangular norm and triangular co norm. Russo proposed a new class of noise-protected operators for edge detection, based on the Fuzzy Inference Ruled by Else-action (FIRE) [14, 15]. Other significant fuzzy approaches to edge detection and contour extraction include weighted fuzzy morphological filtering [16], minimizing the fuzzy entropy criterion [17] and shell clustering [18]. Advanced fuzzy enhancement algorithms based on the gray level fuzzy sets are in existence, for instance, the one driven by complex transformation of the fuzzy space [19]. Jinbo and Zhouping [20] proposed a fast multilevel fuzzy edge detection algorithm for blurry images. The algorithm extracts information for some edges at the expense of other edges. However, changing lighting conditions in noisy images may render this method useless. Chen and Chen [21] found a solution for such problems using the optimal thresholding and fuzzy entropy.

Most of the fuzzy enhancement edge detectors fail in detecting weak or poorly illuminated edges in images. While the Shannon entropy is a measure of the randomness associated with a random variable, the fuzzy entropy realizes the concept of entropy by using fuzzy sets, thus, containing possibilistic uncertainties instead of the probabilistic ones. In this article we attempt to optimize the fuzzy entropy value together with the sharpness factor of the image by controlling the noise content in the image while still preserving the necessary information content in the image. Our edge detection approach employs a recently proposed and very promising metaheuristic algorithm for optimization in real parameter space, called the Gravitational Search Algorithm (GSA) [22]. GSA has already found interesting applications in derivative free optimization of non-linear functions [22], parameter identification [23], power dispatch [24], Takagi-Sugeno fuzzy model identification [25] and so on.

Our approach starts with the computation of USAN area which serves as a measure of the number of pixels having the same gray level as that of the centre pixel. The spatial domain image is transformed into its USAN area equivalent whose histogram has the USAN area as the x-axis and the frequency of occurrence of USAN area along the y-axis. A histogram-based Gaussian function is used to fuzzify the USAN area, giving us the membership values to detect the strong edges. A bell-shaped function, acting as a hedge, is used to detect the weak edges. The shape and range of the bell-shaped function is controlled by three parameters that are used to yield the fuzzy entropy values of the image, which, in turn, are optimized by GSA. Thresholding is applied on the fuzzified USAN area image to get the edge map. A single global threshold gives poor results and to take care of the variations in the USAN area image, locally driven adaptive thresholding is employed.

The organization of the paper is in order. Section IIA introduces the SUSAN principle for the calculation of USAN area. Section IIB describes the fuzzification of USAN area using fuzzy membership functions while Section IIC gives an overall view of the entire optimal fuzzy based algorithm. Section IID introduces the fuzzy measures required to evaluate the fuzzy entropy and sharpness factor of the fuzzy edge map. The GSA algorithm is presented in Section IIE, with the objective function introduced in Section IIF, while in Section IIG, the need for adaptive thresholding is emphasised. Section III presents the experimental results along with the discussions on their qualitative and quantitative analyses. Section IV highlights a few special features of the proposed algorithm. Finally Section V concludes the paper, unearthing some interesting future research issues. The quantitative measures include Shannon's Entropy, Pratt's Figure of Merit, Root Mean Square Error (ERMS), Signal to Noise Ratio (SNR), and Localization Error (LE in %). The performance of the GSA based fuzzy edge detector remains commendable for both colour and grayscale images and even under poor lighting conditions.

IIA. Computation Of SUSAN Area

SUSAN area principle [6] has been invoked in computing the USAN area of the circular mask as shown in Fig.1. The gray levels of the neighbouring 36 pixels are compared with the intensity of the centre pixel using the comparing equation and the outputs are summed up to obtain the USAN area. The concept of each image pixel, having associated with it a local (USAN) area of similar brightness, forms the basis for the SUSAN principle.

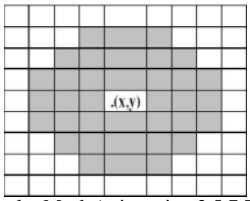

Fig.1: Circular Mask (orientation 3,5,7,7,7,5,3 pixels)

When it is required to compare the two pixels, another parameter (for the brightness of the threshold) '*t*' is required to produce a reasonable output. In general cases the value of *t* is taken to be 20. The USAN area reaches maximum value when the mask is present on a flat portion and becomes half of the maximum at a very near straight edge. Being non-linear and having the summing up effect, USAN principle is likely to perform well on noisy images [6].

The comparison of any pixel with the centre pixel can be quantized as:

$$F(r, r_o) = exp\left[\left(\frac{(-(I(r)-I(r_o))}{t}\right)^6\right], \qquad (1)$$

where r is the position of any pixel, r_o is the position of the centre pixel, $I(r)$ is the intensity of any pixel, $I(r_o)$ is the intensity of the centre pixel and t is the threshold brightness. Eq. (1) is applied on each pixel within the mask and the sum of the outputs is computed as:

This article has been accepted for publication in a future issue of this journal, but has not been fully edited. Content may change prior to final publication. Citation information: DOI 10.1109/TFUZZ.2013.2286418, IEEE Transactions on Fuzzy Systems

$$k(r_o) = \sum_r F\,(r, r_o). \qquad (2)$$

This k (r_o) gives the USAN area of the centre pixel at the position r_o and may vary from 1 to 37.

IIB. Fuzzification Of USAN Area

The probability of an USAN area with a particular number of pixels is calculated as below:

$$p(k) = h(k)/\sum h\,, \qquad (3)$$

where k varies from 1 to 37, $p(k)$ is the frequency of occurrence of area k and $h(k)$ is the total number of pixels having area k, with $p(k)$ satisfying the condition:

$$\sum_{k=0}^{L-1} p(k) = 1, \qquad (4)$$

where L is the total number of pixels in the circular mask i.e. in this case 37. Fuzzy memberships indicate how strongly a gray level belongs to the background or to the foreground. These membership functions convert the intensity values in the spatial domain into fuzzy membership values in the range 0 to 1 and here it is done with the help of Eqn. (5) which represents a histogram based Gaussian membership function:

$$\mu_1(k) = exp\left(-\left(\frac{(xmax-k)^2}{2*{f_h}^2}\right)\right) \qquad (5)$$

The fuzzifier parameter 'f_h' is calculated in the following way:

$${f_h}^2 = \frac{\sum_{k=0}^{L-1}(xmax-k)^4 * p(k)}{2*\sum_{k=0}^{L-1}(xmax-k)^2 * p(k)}. \qquad (6)$$

Here *xmax* is the maximum USAN area and L is 37 as stated before.

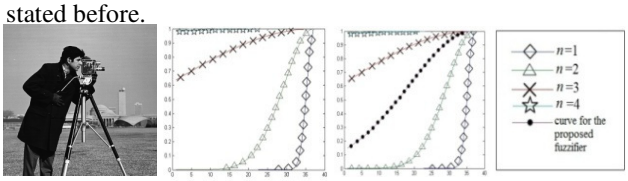

(a) (b) (c) (d)

Fig. 2: (a) cameraman test image (b) The four curves of $\mu_1(k)$ vs.k for n = 1, 2, 3, 4 (c) The four curves of Fig. 2(b) along with an additional curve corresponding to ${f_h}^2 = \frac{\sum_{k=0}^{L-1}(xmax-k)^4 * p(k)}{2*\sum_{k=0}^{L-1}(xmax-k)^2 * p(k)}$ i.e. Eq. (6).

The n-th order partial moment for the discrete variable k with *xmax* as reference point is given by:

$$F(n) = \sum_{k=0}^{L-1}(xmax - k)^n * p(k). \qquad (7)$$

$F(n)$ serves as a measure of deviation of the discrete variable k from *xmax*. Now, let us consider the cameraman test image (shown in Fig. 2(a)) for explaining the mathematical modelling of the fuzzifier f_h. The fuzzifier serves as a measure of the spread of the Gaussian membership function $\mu_1(k)$, used for fuzzifying the USAN area values, varying from 1 to L-1. Fig. 2(b) shows the four curves of $\mu_1(k)$ verses k for n = 1, 2, 3, 4. Evidently, the $\mu_1(k)$ curves assume the shape of half of a Gaussian membership function and provide the fuzzified USAN area values for all k < *xmax*.

The curve (**for *n* = 1**) corresponds to a very low fuzzifier value of $f_h = \sqrt{F(1)}$ = 1.6808, as a result of which the $\mu_1(k)$ values for k < 30 practically reduce to zero, thus leading to poor extraction of the weaker features corresponding to pixels having USAN area k < 30. The curve (**for *n* = 2**) corresponds to a moderately low fuzzifier value of $f_h = \sqrt{F(2)}$ = 7.6306, as a result of which the $\mu_1(k)$ values for k < 10 practically reduce to zero, thus leading to poor extraction of the weaker features corresponding to pixels having USAN area k < 10. The curve (**for *n* = 3**) corresponds to a moderately high fuzzifier value of $f_h = \sqrt{F(3)}$ = 37.9997, as a result of which the spread of $\mu_1(k)$ curve is quite large. Hence the weaker features cannot be differentiated from the stronger features as regions in the image having different pixel intensities cannot be distinguished properly from each other. The curve (**for *n* = 4**) corresponds to an unacceptably high fuzzifier value of $f_h = \sqrt{F(4)}$ = 199.5007 that results in a huge spread of the $\mu_1(k)$ curve. Consequently the edges in the image (which are basically boundaries separating two regions of different pixel intensities) cannot be properly extracted owing to the low differences in their USAN areas. Further utilities of the fuzzifier are analysed in Section IIE. Thus, all the curves in Fig. 2(b) are inappropriate for the fuzzification process. Our main purpose is to fuzzify the USAN area in such a way that the $\mu_1(k)$ values are non-zero for all values of k and spread over half of an appropriately shaped Gaussian membership function, thus facilitating proper differentiation between homogeneous and inhomogeneous regions in the image. Hence the proposed fuzzifier plot shown in Fig. 2(c) with f_h calculated in accordance with Eq. (6) serves our criteria. A bell shaped function meant to enhance the membership function values of the original gray levels of the image can be expressed as:

$$\mu_2(k) = \frac{1}{\left(1+\frac{|\mu_1(k)-a|^{2b}}{c}\right)}, \qquad (8)$$

where a is the centre of the curve, b controls the slope of the curve $\mu_2(k)$ (at $\mu_1(k) = a$-c and $\mu_1(k) = a$+c), and c controls the width of the curve at $\mu_2(k) = 0.5$. These parameters *a, b*, and *c* can be changed as per the user and this makes the fuzzification process more flexible.

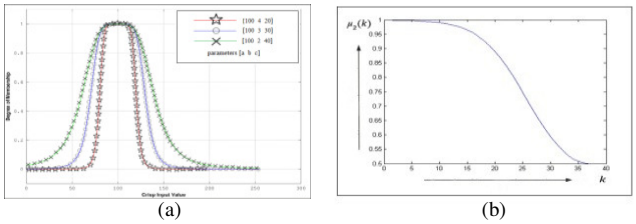

(a) (b)

Fig. 3: (a) Three bell-shaped curves centred at a = 100 but with different values of b and c (b) Shape of $\mu_2(k)$ obtained for the cameraman test image resembles half of a bell-shaped curve. Since the shape of $\mu_1(k)$ is half of a Gaussian membership, its enhanced form $\mu_2(k)$ also assumes a similar shape.

Proper fuzzification is attained only when the weak edge membership values are properly enhanced over the bell-shaped membership function and the overall edge quality is improved. For this reason, certain specific fuzzy measures, depending on the parameters *a, b, c*, and f_h are

This article has been accepted for publication in a future issue of this journal, but has not been fully edited. Content may change prior to final publication. Citation information: DOI 10.1109/TFUZZ.2013.2286418, IEEE Transactions on Fuzzy Systems

evaluated, and fuzzy entropy and edge sharpness factor are optimized together to yield the optimal values of the four parameters.

IIC. An Overview Of The Entire Optimal Fuzzy Based Algorithm

Before introducing the fuzzy measures for developing the mathematical model of the optimal fuzzy algorithm, a flow chart is presented in Fig. 4 to provide an overview of the algorithmic steps.

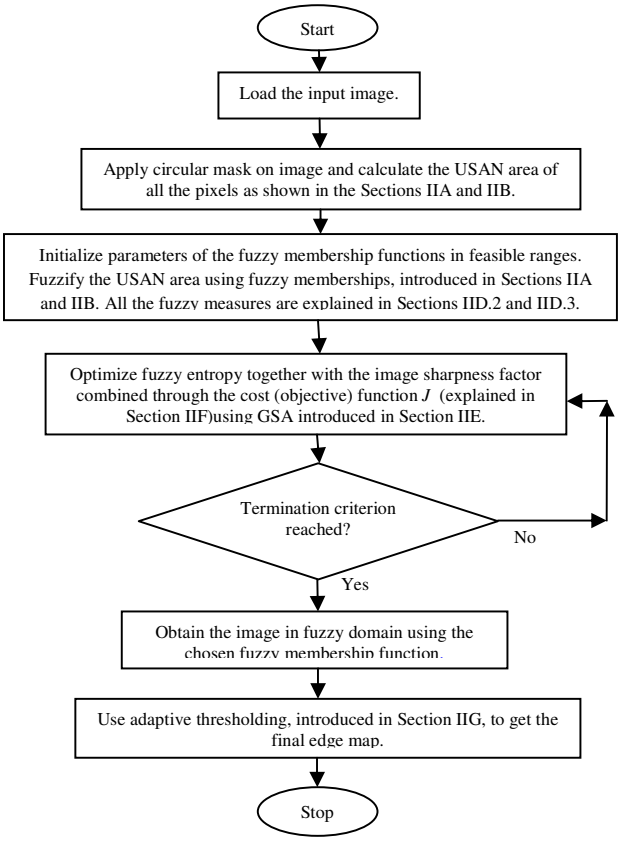

Fig. 4: Flow chart of the proposed approach

Our approach starts by computing the USAN area for each pixel in a test image and for that, a circular mask of 37 pixels is used, in accordance with the SUSAN principle. The USAN area values, thus obtained, are fuzzified using fuzzy membership functions and optimal fuzzification is attained only after optimizing the fuzzy entropy together with the sharpness factor of the fuzzy edge map. Our algorithm uses GSA as the core optimizer to attain optimal values of the parameters that control the range and shape of the membership curve and ultimately produce optimal values for the fuzzy entropy and sharpness factor, which together constitute the objective function. Once the GSA iterations are terminated (based on some standard stopping criteria in evolutionary computing community, like the exhaustion of a predefined number of objective function evaluations), an adaptive thresholding is applied on the optimal fuzzy edge map to attain the final edge map. For a colour image, the entire procedure is repeated for all three RGB components and the resultant edge maps are concatenated to produce the final edge map.

IID.1. Fuzzy Measures

In our algorithm, the fuzzy measures used include different fuzzy sharpness factors for edges. These measures are introduced to compute the objective function and sharpen different edges. A fuzzy sharpness factor helps to determine the quality of different edges, along with entropy, thereby serving as a metric by which strong edges can be distinguished from weak edges. The fuzzy edge sharpness factors are basically measures to calculate deviations of the membership values from the crossover point of the bell-shaped membership function. There may be two fuzzy edge sharpness factors- one to determine strong edges and the other to determine weak edges.

The fuzzy edge sharpness factor for the weak edges can be formulated as:

$$F_w = \frac{1}{L}\sum_{k=0}^{L-1}\left(\mu_2(k) - c\right)^2 * p(k). \quad (9)$$

The average fuzzy edge sharpness factor for the weak edges can be formulated as:

$$F_{avgW} = \frac{1}{L}\sum_{k=0}^{L-1}(\mu_2(k) - c) * p(k). \quad (10)$$

The fuzzy edge sharpness factor for the strong edges can be formulated as:

$$F_S = \frac{1}{L}\sum_{k=0}^{L-1}\left(\mu_1(k) - c\right)^2 * p(k). \quad (11)$$

The average sharpness factor for the strong edges can be formulated as:

$$F_{avgS} = \frac{1}{L}\sum_{k=0}^{L-1}(\mu_1(k) - c) * p(k). \quad (12)$$

The average fuzzy edge sharpness factors indicate the overall sharpness of an image, whereas the individual fuzzy sharpness factors determine the actual deviations from the crossover point (here denoted by *c*).

A fuzzy edge quality factor is formed by taking the ratio of the average to the actual value of the fuzzy edge sharpness factors. This quality factor determines the uncertainty present in the edges. The fuzzy edge quality factor for weak edges is denoted by:

$$Q_W = \frac{F_{avgW}}{F_w}. \quad (13)$$

The fuzzy edge quality factor for strong edges is denoted by:

$$Q_S = \frac{F_{avgS}}{F_s}. \quad (14)$$

IID.2. Fuzzy Entropy

In accordance with Shannon's theorem, entropy is the average amount of information present in an image. However venturing into the fuzzy domain, this definition is slightly modified [26]. Here entropy becomes a measure of the uncertainty or randomness associated with the image information and is defined as:

$$E = \frac{-1}{L*ln2}\sum_{k=0}^{L-1}\left[\mu_2(k) * \ln\left(\mu_2(k)\right) + \left(1-\mu_2(k)\right) * \left(\ln\left(1-\mu_2(k)\right)\right)\right]. \quad (15)$$

This article has been accepted for publication in a future issue of this journal, but has not been fully edited. Content may change prior to final publication. Citation information: DOI 10.1109/TFUZZ.2013.2286418, IEEE Transactions on Fuzzy Systems

Fuzzy entropy is a measure of the amount of information that can be extracted from an image. It is intuitively apparent that lesser information is required to distinguish a weak edge from a noisy pixel than that is required to determine a strong edge. Hence, optimizing the entropy value is of utmost importance as this will help to determine the optimal values of the parameters: a, b, c, and f_h .

IID.3. SHARPNESS FACTOR

The normalized fuzzy edge sharpness factor is required to calculate the fuzzy edge sharpness. The sharpness factor is defined as:

$$S_f = \frac{Q_S}{Q_W}. \tag{16}$$

This definition helps us to fix a limit for the fuzzy edge sharpness factor, because increasing its value beyond the limit would cause the loss of edge information. Experimentally, for a good edge map, the value of the sharpness factor should be in the range 1 to 1.5.The concept of sharpness factor of an edge map is introduced so that sharpening of the SUSAN based USAN area edges are possible by regulating this factor. Sharpening of edges basically refers to improvement in edge quality. A detailed analysis about the utility of this factor is done later in Section III with the aid of Fig. 5 and we shall arrive at it subsequently.

IIE.GRAVITATIONAL SEARCH ALGORITHM (GSA)

Over the past few decades, a number of derivative free optimization algorithms, inspired by various natural phenomena, have been developed and applied to solve mathematically intractable real world problems from diverse domains of science and technology. Various metaheuristic algorithms are in existence but no particular algorithm yields the best solution for all possible optimization problems. A novel stochastic optimization algorithm called GSA, has been recently proposed, based on the Newton's gravitational law which states that every particle in the universe attracts every other particle with a force whose magnitude is directly proportional to the product of their masses and inversely proportional to the square of the distance between them. The force between a pair of mass particles may be expressed as:

$$F=GM_1M_2/R^2, \tag{17}$$

where F is the magnitude of the gravitational force, G is the gravitational constant (decreasing with earth's age), $M_1$and M_2 are the masses of the first and second particles respectively and R is the distance between them.

In GSA, the population members or agents are considered as objects and the heaviest object corresponds to the best solution. A heavier object corresponding to a better solution moves slowly with respect to the lighter objects whereas objects with lesser mass are drawn faster towards the heaviest object, thereby satisfying the criterion of optimization.

In GSA [22], an agent or mass is specified by its position, inertial mass (M_i), active gravitational mass (M_a) and passive gravitational mass (M_p).

Inertial Mass (M_i) of an object is the resistance it offers to the changing of its state of motion under the application of an externally applied force.

Active Gravitational Mass (M_a) is the strength of the gravitational field due to a particular object.

Passive gravitational mass (M_p) is the strength of an object's interaction with the gravitational field.

The algorithm design starts with the identification and randomized initialization of the search agents (trial solutions or particles) in a feasible search space. The position of the i-th agent of the N-sized population is given by:

$$X_i = \left(x_i^1, \ldots., x_i^d, \ldots., x_i^n\right), \tag{18}$$

for i = 1, 2, 3, … ,N, where x_i^d represents d-th dimension of the position vector of the i-th object. Next the fitnesses of the agents are evaluated by using the objective function which, in this case, comprises of the entropy and edge sharpness factor optimizer J and is defined subsequently. Gravitational and inertial masses are updated and $best(t)$ and $worst(t)$ of the population are evaluated by the following equations:

$$M_{ai} = M_{pi} = M_{ii} = M_i, \qquad \text{for } i = 1, 2, 3\ldots.N. \tag{19}$$

$$m_i(t) = \frac{fit_i(t)-worst(t)}{best(t)-worst(t)}. \tag{20}$$

$$M_i(t) = \frac{m_i(t)}{\sum_{j=1}^{N} m_j(t)}. \tag{21}$$

$$best(t) = \min_{j\in\{1,\ldots,N\}} fit_j(t). \tag{22}$$

$$worst(t) = \max_{j\in\{1,\ldots,N\}} fit_j(t). \tag{23}$$

The agent yielding the least value of the objective function is considered as the fittest in this case as entropy has to be optimized. The gravitational constant $G(t)$ is updated iteratively as:

$$G(t) = G_o \exp\left(\frac{-\beta.t}{t\_max}\right) \tag{24}$$

where G_o is the initial value of the gravitational constant, β is a constant that determines the rate of decrease of G with iterations, t refers to the t-th iteration and t_max refers to the maximum number of iterations.

The force acting between the i-th and j-th agents at the d-th dimension is given in accordance with Newton's law of gravity as:

$$F_{ij}^d(t) = G(t)\frac{M_{pi}(t)\times M_{aj}(t)}{R_{ij}(t)+\varepsilon}\left(x_j^d(t) - x_i^d(t)\right), \tag{25}$$

where M_{aj} is the active gravitational mass of the j-th object, M_{pi} is the passive gravitational mass of the i-th agent, $G(t)$ is the Gravitational constant at time t, ε is a small constant, and $R_{ij}(t)$ is the Euclidian distance between i-th and j-th agents. A stochastic characteristic is given to the algorithm by expressing the total force acting on the i-th particle at the d-th dimension as a randomly weighted sum of the d-th components of forces exerted by other agents:

$$F_i^d(t) = \sum_{j=1, j\neq i}^{N} (rand_j F_{ij}^d(t)), \tag{26}$$

This article has been accepted for publication in a future issue of this journal, but has not been fully edited. Content may change prior to final publication. Citation information: DOI 10.1109/TFUZZ.2013.2286418, IEEE Transactions on Fuzzy Systems

where $rand_j$ is a random number from the interval [0, 1]. The performance of GSA can be improved by modifying Eq. (24) in such a way that only the first K agents ($1 \leq K \leq N$) with the best fitness attract the other agents. Initially, all agents exert force but gradually the *Kbest* value linearly decreases so that only one agent i.e. the heaviest agent exerts force in the final iteration.

$$F_i^d(t) = \sum_{j \in Kbest, j \neq i}^{N} (rand_j F_{ij}^d(t)), \quad (27)$$

Acceleration and velocity can be calculated as follows:

$$a_i^d(t) = \frac{F_i^d(t)}{M_{ii}(t)}, \quad (28)$$

$$v_i^d(t+1) = rand_i \times v_i^d(t) + a_i^d(t). \quad (29)$$

Next, the position of the i-th agent at the d-th dimension at time (t+1) is updated as:

$$x_i^d(t+1) = x_i^d(t) + v_i^d(t+1) \quad (30)$$

A complete pseudo-code of the GSA algorithm is provided as Algorithm 1.

Algorithm 1: Steps of the Gravitational Search Algorithm
Step 1. Initialize the search space, $X_i = (x_i^1, \ldots, x_i^d, \ldots, x_i^n)$.
Step 2. Calculate the fitness of every agent.
Step 3. Update $G(t)$, *best*(t), *worst*(t), and $Mi(t)$ for i=1,2,3,…N.
Step 4. Calculate the total force acting on each agent, given by $F_i^d(t) = \sum_{j \in Kbest, j \neq i}^{N} (rand_j F_{ij}^d(t))$ for every i-th agent.
Step 5. Update the velocity and position of each agent.
Step 6. Repeat steps 2–5 until the stopping criterion is reached.

The main parameters of GSA are G_o, β and the population size. The values of these parameters are dependent on the size of the search space. We employed the standard parametric settings for GSA as prescribed in [22], with G_o fixed to 1 and β equal to 0.1. The population size was kept at 30. The same parametric setup was employed for all the images tested and it provided acceptably well solutions for all test cases. In our proposed algorithm, each of the GSA agents or masses is represented as:

$$X_i = [\, a_i, b_i, c_i\, f_{h_i} \,]^T. \quad (31)$$

The objective function for optimization is explained in Section IIF.

IIF. Objective Function For Optimization

Fuzzy entropy is a function of fuzzy sets that becomes lesser when the sharpness of the argument fuzzy set is improved. The entropy as well as the edge sharpness factor determines edge quality. So their simultaneous optimization is necessary. The entropy function E, presented already in Eq. (15) is optimized subjected to the constraint:

$$S_{df} = S_f. \quad (32)$$

For this, an objective function J is defined following the aggregate sum method as:

$$J = E + \lambda * |S_{df} - S_f|. \quad (33)$$

Evidently J is a function of the parameters *a, b, c* of the bell-shaped curve $\mu_2(k)$ and the fuzzifier f_h of the Gaussian membership $\mu_1(k)$ and hence optimization of J is attained by regulating *a, b, c*, and f_h. The value of λ, introduced in Eq. (33), is chosen to be 0.5. Feasible search ranges for the optimization parameters were experimentally chosen as $-4 < a < 0$; $1 < b < 6$; $1 < c < 4$. Optimization was carried out using GSA, where *a, b, c* parameters of the chosen 30 member population were initialised subject to the set of constraints presented above. The fuzzifiers f_h for the USAN area edge maps of all the test images, prior to the optimization of the objective function J, were found to be in the range of 15 to 22. The USAN area maps, prior to optimization, have both unregulated noise and thick edges. After optimizing the fuzzy entropy together with the sharpness factor, the *a*, *b*, *c* parameters were fixed to their optimal values (presented later in Table 2) and the fuzzifier value f_h was varied from 0 to 60. Figures 5(a)-(g) qualitatively show the edge maps for varying f_h while Fig. 5(h) shows the variation of the sharpness factor (S_f) with fuzzifier (f_h). A low value of f_h, generally below 5, corresponds to extremely thick edges while a high value, typically beyond 60, leads to loss of information as is evident from Fig. 5 which shows the fuzzified USAN area edge maps of the cameraman test image for different values of f_h ranging from 0 to 60. The best result was attained at the optimal value of f_h = 20.2178, shown in Fig. 5(d). Thus the f_h values of all the population members were initialized within 5 to 60. Please note that these are fuzzy edge maps and the analysis has been done prior to adaptive thresholding which is applied later to yield the final edge maps.

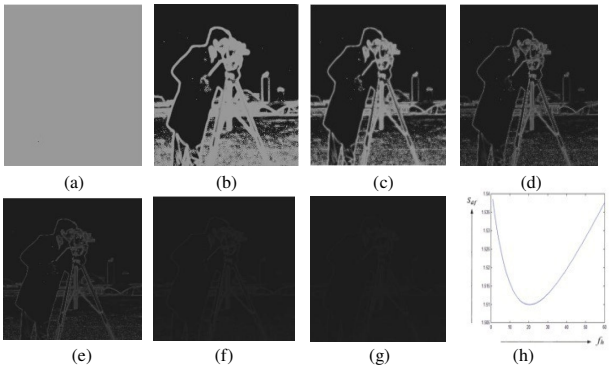

Fig. 5: (a) USAN area map fuzzified with f_h = 0 (b) f_h = 5 (c) f_h = 10 (d) optimal fuzzy edge map (f_h = 20.2178) (e) f_h =30 (f) f_h = 50 (g) f_h = 60 (h) variation of sharpness factor (S_f) with fuzzifier (f_h).

It is evident from the plot in Fig. 5(h) that the sharpness factor S_f is closest to the desired sharpness value S_{df} =1.5 at the optimal value of f_h=20.2178. Precisely, S_f=1.5045 at f_h =20.2178. For other values of f_h, the sharpness factor is found to increase from the desired value i.e. 1.5. Now increased values of S_f beyond the desired limit can occur due to two reasons:

a) For f_h**< 20.2178**, the strong edges get thicker and blurry as is evident from Figs. 5(a), (b),(c). Despite low values of Q_S (corresponding to thicker and blurry strong edges),the ratio $S_f = \frac{Q_S}{Q_W}$ still yields higher values than the desired

This article has been accepted for publication in a future issue of this journal, but has not been fully edited. Content may change prior to final publication. Citation information: DOI 10.1109/TFUZZ.2013.2286418, IEEE Transactions on Fuzzy Systems

limit as the Q_w values are still extremely low compared to the low Q_s values. Evidently, f_h =0 corresponds to the infinitely thick and blurry strong edges and hence, Fig. 5(a) appears greyish.

b) For f_h**> 20.2178**, Q_S or the strong edge quality factor exceeds Q_W i.e. the weak edge quality factor, by an appreciable margin, thereby leading to almost complete suppression of weak edge information (due to low Q_w) and excessive sharpening of the strong edges (due to high Q_s). This is evident from Figs. 5(e), (f), (g) where excessive sharpening of the strong edges has lead to loss of edge information.

IIG. Adaptive Thresholding

Bi-level image thresholding [27, 28], be it global or local, usually takes a grayscale image as input and produces a binary image as output. Global thresholding processes compute a global threshold value for the entire grayscale image which demarcates between the foreground and the background pixels. However, an image may have spatial variations in illumination and in such cases, the threshold has to be dynamically varied over the image. This process may be carried out either by the Chow and Kaneko method [27] or simply by local thresholding. The Chow and Kaneko method divides the image into a number of sub-images and calculates the threshold for the individual sub-images. Finally it interpolates the results of the sub-images to determine the threshold for each pixel. Local thresholding (as has been applied to our algorithm) investigates the neighborhood of each pixel and statistically determines the threshold for each pixel. The statistic used may be mean, median or mean of the maximum and minimum intensity values in the neighborhood. The statistic used in thresholding the fuzzy domain edge maps to obtain the final edge maps in our case was mean. Fig. 6 shows the result of a local adaptive thresholding on an image having variable spatial illumination.

In case of color images, adaptive thresholding is applied to the optimal fuzzy edge maps to obtain the spatial domain image edge maps for the Red (R), Green (G), and Blue (B) components separately, which are then finally concatenated to produce the final image edge map. In case of grayscale images, however, this concatenation is not required.

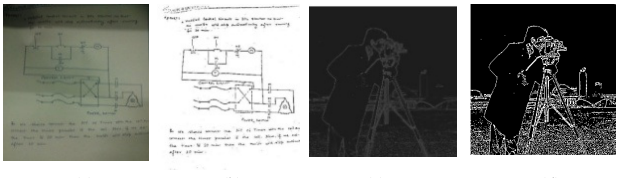

(a) (b) (c) (d)

Fig.6: a) An image having changing lighting conditions b) Image obtained after application of local adaptive thresholding c) The optimal fuzzy edge map for cameraman test image having spatial variations d) Final edge map optained after adaptive thresholding of the optimal fuzzy edge map.

The termination criterion can be the exhaustion of a pre-fixed number of objective Function Evaluations (FEs) following the standard of the evolutionary computing research.

III. Experimental Results

The proposed approach has been evaluated on well-known test images of varying levels of complexities and its performance was analyzed with respect to existing as well as state-of-the-art edge detection schemes. Fig. 7 presents the nine test images and Fig. 8 shows the final RGB edge map and the individual RGB edge maps of the test image Lena. Figs. 7(f) and 7(g) have been taken from the Berkeley Segmentation Data Set (BSDS) (http://www.eecs.berkeley.edu/Research/Projects/CS/vision/bsds). Table 1 shows the optimal values of the parameters *a, b, c*, and f_h for the RGB edge maps of Lena test image.

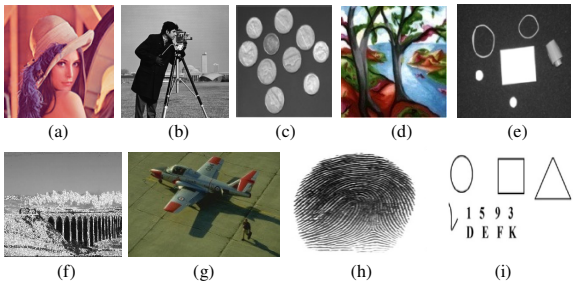

(a) (b) (c) (d) (e)

(f) (g) (h) (i)

Fig. 7: Original test images (a) Lena (b) Cameraman (c) Coins (d) Trees (e) Pillsetc (f) Smoke (g) Plane (h) Fingerprint (i) Shapes

(a) (b) (c) (d)

Fig.8:(a) Final RGB edge map (b) R component edge map (c) G component edge map (d) B component edge map

Table 1: RGB optimized values (Using GSA) for Lena

Parameters	RED	GREEN	BLUE
a	-2.000	-2.000	-2.000
b	3.0006	3.0004	3.0011
c	2.2763	2.2583	2.2951
f_h	23.6190	23.1441	24.6299

III A. Qualitative Comparisons

Figs. 9 - 11 provide a qualitative analysis of the edge maps of three of the nine test images (Lena, Pillsetc, and Cameraman respectively) with respect to traditional as well as recently developed edge detectors. The traditional ones include the Canny, Edison, Rothwell, LoG, SUSAN, Roberts, and Sobel while the recently developed edge detection algorithms [33, 36] include a Bacterial Foraging Algorithm (BFA) [31] based scheme [33] that also incorporates a probabilistic derivative technique derived from the Ant Colony Systems (ACS) [32] and another edge detection scheme [36] based on the energy and skewness features of an image. The algorithm proposed in

This article has been accepted for publication in a future issue of this journal, but has not been fully edited. Content may change prior to final publication. Citation information: DOI 10.1109/TFUZZ.2013.2286418, IEEE Transactions on Fuzzy Systems

[36] has found application in detecting fat layer in meat. Differential Evolution (DE) [29] and Particle Swam Optimization (PSO) [30] were also used as optimizers, with standard parameter sets, in place of GSA under our proposed fuzzy method for edge detection and their performances have been compared with the GSA based fuzzy approach. Table 2 presents the GSA optimal values of the parameters *a, b, c,* and f_h for Pillsetc and Cameraman test images.

Table 2: Optimized values(using GSA) for Pillsetc and Cameraman images

Parameters	Optimal Values	
	Pillsetc Image	Cameraman Image
a	-2.000	-2.000
b	3.0010	3.0001
c	2.3295	2.1013
f_h	26.5178	20.2178

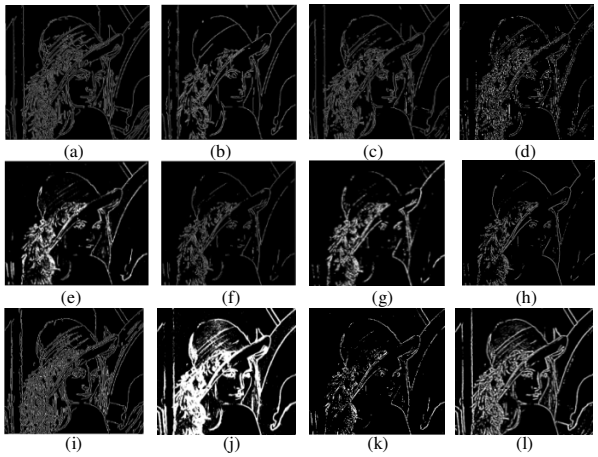

Fig. 9:(a) Canny(b) Edison(c) Rothwell(d)LoG (e)SUSAN (f) Roberts (g) Sobel(h) BFA based edge detector [33] (i)Edge detector of [36] (j)Optimal Fuzzy(DE) (k)Optimal Fuzzy(PSO) (l)Proposed Method (Optimal Fuzzy(GSA))

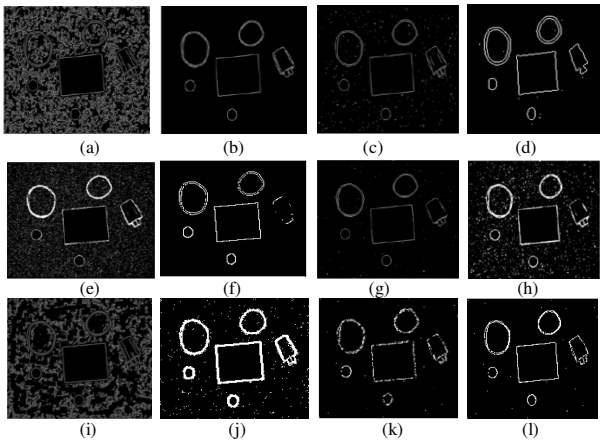

Fig. 10:(a) Canny (b) Edison(c) Rothwell(d) LoG (e) SUSAN (f) Roberts (g) Sobel (h) BFA based edge detector [33] (i) Edge detector of [36] (j) Optimal Fuzzy(DE) (k) Optimal Fuzzy(PSO) (l)Proposed Method(Optimal Fuzzy(GSA))

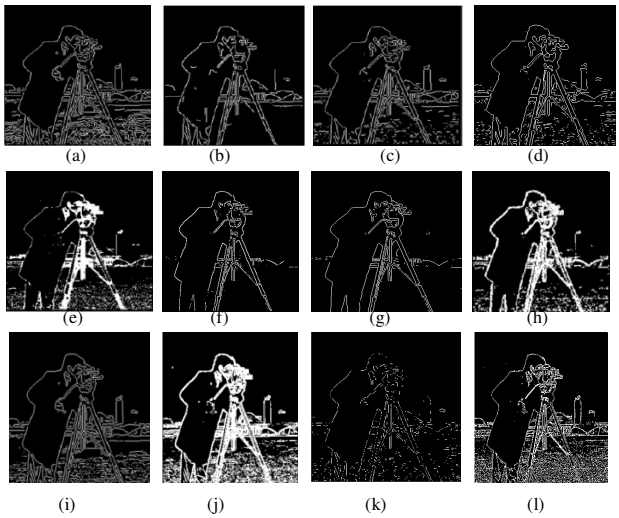

Fig. 11:(a) Canny(b) Edison(c) Rothwell(d) LoG (e) SUSAN (f) Roberts (g) Sobel(h) BFA Based Edge Detector (i) Edge detector of [36] (j)Optimal Fuzzy(DE) (k) Optimal Fuzzy(PSO) (l)Proposed Method (Optimal Fuzzy(GSA))

Figs. 9-11 indicate that the optimal fuzzy edge detector using GSA performs better than the other edge detectors. Optimal fuzzy edge detection system using PSO in place of GSA and the BFA based edge detection scheme of [33] fail as weak-edge detection schemes as is evident from the superior weak-edge detection in the optimal fuzzy GSA approach. For instance in Fig.9, the weak edges to the rightmost bottom corner, the leftmost upright structure, etc. are almost indeterminable in the PSO (Fig.9(j)) and BFA based systems (Fig.9(h))while they are almost clearly visible in the fuzzy GSA edge map (Fig.9(k)). The PSO and BFA based spatial edge maps show weak edge connectivity and inability to detect the weak edges completely. On the other hand, the DE-based spatial domain edge maps(Figs. 9(i), 10(i), 11(i)) show greater noise content and thicker edges and hence this method shows no significant improvement over the SUSAN (Figs. 9(e), 10(e), 11(e)) method of edge detection. As is evident from the experimental results, the performance of the GSA based fuzzy edge detector remains commendable for all the test images and as compared to the other metaheuristic based fuzzy and non-fuzzy algorithms.

As for the traditional edge detectors, Canny [4, 5] and Edison edge detectors produce double edges and distort the shape of the image while Rothwell, LoG, and SUSAN [6] show greater noise content, with the SUSAN edge maps also having weak edge connectivity. Roberts and Sobel detect minimum number of edges among all these edge detectors. The edge detector of [36] produces unwanted double edges. The optimization of fuzzy entropy using GSA not only helps to regulate noise content but also assigns optimal membership values to both weak and strong edges such that even the relatively weaker edges can be distinguished through adaptive dynamic thresholding. Thus, the optimized parameters of the bell-shaped curve and the

This article has been accepted for publication in a future issue of this journal, but has not been fully edited. Content may change prior to final publication. Citation information: DOI 10.1109/TFUZZ.2013.2286418, IEEE Transactions on Fuzzy Systems

optimal value of the fuzzifier help to detect the weak edges in the image. Hence our proposed edge detection approach preserves the unique characteristics of each image without distorting it and also serves as a good detector of weak edges.

III B. Quantitative Analysis

In this section the proposed edge detection scheme has been evaluated on the basis of a number of quantitative measures. Note that the quantitative measures for all metaheuristic algorithms were calculated after averaging through 25 independent runs of each algorithm for each image, each run being continued till 60,000 function evaluations.

IIIB.1 Kappa Value

Kappa value [34] of an image with respect to a ground truth or majority image is a measure of its pixel-to-pixel similarity with the truth image. A majority or truth image in our case has been formed from the edge maps obtained by using Canny, Edison, Rothwell, LoG, Roberts, Sobel and SUSAN. A ground truth pixel will be an edge pixel if majority of the edge detectors mentioned above produce an edge pixel at that coordinate. Table 3 shows the Kappa Values of all the edge detectors. Our proposed approach shows maximum truthfulness or maximum agreement with the majority image as is evident from its highest kappa values for all test images. Kappa Value is a statistic given by:

$$Kappa = \frac{Observed\ Agreement - Expected\ Agreement}{1 - Expected\ Agreement}. \quad (34)$$

Table 3: Kappa values for various edge maps. Best results are marked in boldface

ALGORITHM	KAPPA VALUES								
	Lena	Cameraman	Coins	Trees	Pillsetc	Smoke	Plane	Fingerprint	Shapes
Canny	0.4592	0.4174	0.5543	0.5343	0.2243	0.5962	0.5211	0.5362	0.6013
Edison	0.4654	0.4364	0.3654	0.5254	0.5754	0.6001	0.5342	0.5992	0.6113
Rothwell	0.4384	0.5284	0.4984	0.5374	0.5941	0.5982	0.5232	0.5331	0.5775
LoG	0.3872	0.4974	0.5011	0.5115	0.5621	0.5741	0.4566	0.5221	0.5862
SUSAN	0.4250	0.5564	0.4680	0.5184	0.4380	0.5542	0.5213	0.4916	0.5843
Roberts	0.3441	0.3104	0.3291	0.3971	0.4142	0.3217	0.3121	0.3113	0.5785
Sobel	0.3792	0.3242	0.3743	0.4102	0.4292	0.3646	0.3180	0.3423	0.5891
BF based system [32]	0.5125	0.6393	0.5125	0.5784	0.5255	0.5828	0.5186	0.5331	0.6212
Edge detector of [36]	0.4613	0.3977	0.5724	0.5123	0.3546	0.6216	0.5221	0.5992	0.6292
Fuzzy(PSO)	0.4997	0.3167	0.4212	0.4307	0.4017	0.5882	0.5443	0.4765	0.5613
Fuzzy(DE)	0.5433	0.6403	0.4733	0.5641	0.5134	0.5993	0.5626	0.4872	0.5875
Fuzzy(GSA)	**0.6401**	**0.6899**	**0.6594**	**0.6112**	**0.6971**	**0.6771**	**0.6632**	**0.6531**	**0.6727**

IIIB.2 Shannon's Entropy

It is the measure of randomness in an image and is measured by:

$$H(I) = \sum_0^{L-1} p_i * log\ (p_i), \quad (35)$$

where p_i is the probability of occurrence of pixel with intensity i and I is the test image. Shannon's entropy is measured on a scale of 0 to 1. A high value of Shannon's entropy does not necessarily imply high information content. Unregulated noise also contributes to such high values. Thus, it is mandatory to develop an algorithm that can simultaneously regulate noise content as well as retain essential information. Table 4 presents the Shannon's entropy values of the competing edge detectors. Canny and Rothwell produce double edges while LoG and SUSAN edge maps are filled with noise. Hence, as can be observed from Table 4, their entropy values are higher than that corresponding to our proposed approach i.e. optimal fuzzy edge detection system using GSA. The optimal fuzzy edge detection system using DE fails to regulate noise content as is indicated by its higher value of Shannon's Entropy. The BFA based system owes its higher value of Shannon's Entropy to thick edges and unregulated noise as in the case of the Pillsetc image (Fig. 10). Roberts, Sobel, and PSO based fuzzy system detect fewer edges and hence their corresponding edge maps have low information content, reflected by their lower values of Shannon's Entropy. Edison shows lower Shannon's Entropy value than our proposed approach for three test cases (Pillsetc, Cameraman and Coins).

Table 4: Values of Shannon's entropy [7] for various edge maps. Best results are marked in boldface.

ALGORITHM	SHANNON'S ENTROPY VALUES								
	Lena	Cameraman	Coins	Trees	Pillsetc	Smoke	Plane	Fingerprint	Shapes
Canny	0.8848	0.9931	0.9201	0.9109	1.421	0.9223	0.9113	0.9441	0.8824
Edison	0..6777	0.6852	0.4992	0.8682	0.2369	0.6772	0.6622	0.6712	0.5331
Rothwell	0.7438	0.8015	0.7201	1.0936	0.3332	0.8211	0.8361	0.8119	0.8113
LoG	0.8114	0.8604	0.8298	0.8458	0.8871	0.8221	0.7993	0.7922	0.8014
SUSAN	0. 7928	1.1499	0.8759	1.7299	1.1692	0.9912	0.9211	0.9442	0.8992
Roberts	0.5124	0.5226	0.5125	0.5671	0.2112	0.5211	0.4911	0.4991	0.3911
Sobel	0.5303	0.5633	0.4821	0.5791	0.2265	0.5443	0.4663	0.5221	0.4432
BF based system	0.7146	1.2212	0.8600	0.8682	0.7903	0.7224	0.7192	0.7134	0.7412
Edge detector of [36]	0.9119	0.9475	0.8875	0.9213	1.2124	0.9874	0.9442	0.9667	0.9784
Fuzzy(PSO)	0.5464	0.5788	0.6432	0.6221	0.3442	0.5051	0.4331	0.5225	0.5541
Fuzzy(DE)	0.9272	0.9717	0.9554	1.4223	0.7989	0.9882	0.9512	1.2881	0.9883
Fuzzy(GSA)	**0.6631**	**0.6989**	**0.6771**	**0.8221**	**0.4223**	**0.6223**	**0.5912**	**0.6442**	**0.5122**

This article has been accepted for publication in a future issue of this journal, but has not been fully edited. Content may change prior to final publication. Citation information: DOI 10.1109/TFUZZ.2013.2286418, IEEE Transactions on Fuzzy Systems

For the noise-hit Pillsetc image, Edison serves as a good regulator of noise, reflected by its lowest value of Shannon's entropy but it fails to produce weaker edges for the cameraman and coins images.
Thus, the comparison in Table 4 shows the ability of the GSA based fuzzy edge detector to detect weak edges while still managing to regulate the noise content, indicated by its optimal Shannon's Entropy value.

IIIB. 3 PRATT'S FIGURE OF MERIT

Edge detectors may deviate from ideality by failing to satisfy three criteria:

- Detection of all edge points
- Localization of edge points
- Distinguishing noise fluctuations from actual edge points.

Pratt's Figure of Merit **(PFOM)** **[**35] measures the ideality factor of an edge detector on a scale of 0 to 1, based on the criteria stated above. A PFOM value of 1 indicates that the edge map produced by the algorithm perfectly resembles the ideal edge map whereas a PFOM value of 0 refers to complete deviation from ideality. PFOM is mathematically represented as:

$$PFOM = \frac{1}{I_N}\sum_{1}^{I_A}\frac{1}{1+f*d^2} \quad (36)$$

where I_N = max (I_A, I_I), I_A represents the total number of edge pixels in the obtained edge map while $I_I$refers to the edge pixels in the ideal edge map. The scaling factor f is kept at a value of 0.9 where d represents the distance between the actual edge pixel and the nearest ideal pixel. The normalization is done with the maximum of I_A and I_I to take into consideration the penalty that may occur due to smeared $(I_A > I_I)$ or fragmented $(I_A < I_I)$ edges.

Table 5 shows that for all the test cases, our proposed method yields the highest value of PFOM**,** thus behaving as the closest approximate to the ideal edge maps, two of which (smoke and plane) have been taken from the BSDS database. The others have been formed by combining the best features from the edge maps obtained using Canny, Edison, Rothwell, LoG, Roberts, Sobel and SUSAN. Canny and LoG produce too many double edges and hence have low PFOM value. Sobel yields a very low PFOM value as it detects lesser number of edges. While the DE based system fails to regulate noise content, the BFA and PSO based systems show poor edge connectivity and inability to detect weak edges, along with unregulated noise in case of the BFA based system. The optimal fuzzy edge detector (using GSA) has regulated noise and has also succeeded in detecting weak edges, thus justifying the relatively high PFOM of the edge maps.

IIIB.4 OTHER OBJECTIVE MEASURES

1. Global Measures

ERMS and SNR are global objective measures that serve as similarity metrics for the output edge map with respect to the ground truth or majority or exact edge map. These two metrics can be expressed as:

$$ERMS = \sqrt{\frac{1}{M*N}\sum_{x=1}^{M}\sum_{y=1}^{N}[E(x,y) - O(x,y)]^2}. \quad (37)$$

$$SNR = \sqrt{\frac{\sum_{x=1}^{M}\sum_{y=1}^{N}[E(x,y)]^2}{\sum_{x=1}^{M}\sum_{y=1}^{N}[E(x,y)-O(x,y)]^2}}. \quad (38)$$

Here E refers to the exact edge map or the majority edge map and O refers to the output edge map.

2. Localization Error

Localization Error is a local measure that compares the output edge distribution along x and y coordinates with the corresponding exact edge distribution and is shown in Eqn. (39). The average of the localization errors along all the rows and columns yields the net Localization Error (LE).

$$LE = \frac{|\sum pixels\ of\ exact\ edges - \sum pixels\ of\ output\ \ edges|}{N} * 100\% \quad (39)$$

where N is the total number of pixels along the row or column direction i.e. the direction of evaluation.
Table 6 reveals that our proposed approach achieves the lowest ERMS, the highest SNR, and the lowest LE in %

Table 5. Pratt's Figure Of Merit for various edge maps. Best results are marked in boldface.

ALGORITHM	PRATT'S FIGURE OF MERIT								
	Lena	Cameraman	Coins	Trees	Pillsetc	Smoke	Plane	Fingerprint	Shapes
Canny	0.5542	0.4411	0.5221	0.5212	0.2441	0.6022	0.5232	0.5272	0.6112
Edison	0.5461	0.4622	0.3542	0.5266	0.5612	0.6223	0.5441	0.6011	0.6312
Rothwell	0.5184	0.5242	0.4821	0.5437	0.5741	0.5991	0.5112	0.5184	0.5876
LoG	0.4721	0.4847	0.5231	0.4998	0.5512	0.5631	0.4458	0.5114	0.5912
SUSAN	0.5115	0.5634	0.4407	0.4831	0.4414	0.5662	0.5221	0.4955	0.5994
Roberts	0.3592	0.3121	0.3182	0.3771	0.4135	0.3041	0.2991	0.3002	0.5775
Sobel	0.3761	0.3244	0.3651	0.4221	0.4323	0.3156	0.3080	0.3341	0.5889
BF based system [32]	0.4925	0.5812	0.5223	0.5812	0.5264	0.5784	0.4958	0.5251	0.6242
Edge detector of [36]	0.5663	0.4231	0.5761	0.5211	0.4116	0.6114	0.5134	0.6011	0.6343
Fuzzy(PSO)	0.5812	0.3167	0.4311	0.4367	0.4222	0.5883	0.5536	0.4772	0.5642
Fuzzy(DE)	0.5672	0.6403	0.4882	0.5711	0.5124	0.6232	0.5771	0.4856	0.5912
Fuzzy(GSA)	**0.6721**	**0.6794**	**0.6621**	**0.6421**	**0.6571**	**0.6753**	**0.6635**	**0.6441**	**0.6831**

This article has been accepted for publication in a future issue of this journal, but has not been fully edited. Content may change prior to final publication. Citation information: DOI 10.1109/TFUZZ.2013.2286418, IEEE Transactions on Fuzzy Systems

Table 6: ERMS, SNR AND LE% (FROM TOP TO BOTTOM) Best results are marked in boldface.

Test Images	ALGORITHM											
	Canny	Edison	Rothwell	LoG	SUSAN	Roberts	Sobel	BF based [33]	Detector of [36]	Fuzzy PSO	Fuzzy DE	Fuzzy GSA
Lena	0.356 0.512 29.121	0.312 0.556 27.654	0.321 0.533 26.711	0.272 0.592 25.611	0.291 0.537 24.721	0.392 0.457 30.271	0.373 0.492 29.122	0.276 0.588 23.212	0.314 0.547 24.569	0.378 0.527 24.221	0.315 0.542 23.998	**0.212** **0.612** **22.677**
Cameraman	0.331 0.471 25.792	0.342 0.463 27.245	0.257 0.531 24.312	0.301 0.513 25.276	0.261 0.524 24.233	0.397 0.411 32.771	0.351 0.453 29.278	0.272 0.519 25.110	0.292 0.516 24.962	0.392 0.421 31.221	0.254 0.542 26.661	**0.237** **0.575** **21.431**
Coins	0.274 0.537 22.112	0.512 0.314 31.756	0.324 0.476 29.225	0.312 0.492 24.243	0.310 0.502 25.122	0.398 0.421 30.232	0.344 0.453 29.212	0.342 0.464 24.212	0.265 0.552 22.117	0.314 0.488 24.234	0.322 0.461 23.511	**0.253** **0.592** **20.201**
Trees	0.381 0.467 27.297	0.321 0.512 26.311	0.344 0.431 28.111	0.322 0.401 27.654	0.378 0.479 26.212	0.372 0.392 30.242	0.365 0.412 29.271	0.297 0.462 26.271	0.314 0.477 25.445	0.372 0.492 26.212	0.367 0.532 29.414	**0.268** **0.578** **25.221**
Pillsetc	0.414 0.347 31.220	0.312 0.498 29.282	0.397 0.467 28.834	0.412 0.422 31.547	0.388 0.481 29.247	0.434 0.343 34.121	0.398 0.414 32.531	0.437 0.333 29.227	0.352 0.527 30.451	0.422 0.311 27.332	0.392 0.476 28.210	**0.313** **0.514** **26.212**
Smoke	0.312 0.422 27.714	0.291 0.445 26.221	0.322 0.404 28.912	0.294 0.411 27.263	0.304 0.433 28.219	0.315 0.392 31.988	0.307 0.404 29.887	0.298 0.517 28.555	0.277 0.507 26.780	0.301 0.402 30.091	0.288 0.427 28.292	**0.257** **0.592** **25.645**
Plane	0.267 0.412 26.212	0.256 0.434 24.212	0.272 0.392 27.228	0.272 0.422 27.231	0.291 0.413 27.981	0.311 0.362 29.314	0.297 0.391 28.272	0.282 0.512 27.434	0.252 0.497 25.220	0.312 0.377 28.541	0.301 0.421 27.888	**0.232** **0.552** **24.833**
Fingerprint	0.240 0.527 24.277	0.235 0.572 24.071	0.255 0.541 25.221	0.248 0.522 24.553	0.237 0.517 25.337	0.276 0.533 26.212	0.262 0.542 26.112	0.228 0.537 27.233	0.236 0.561 23.373	0.244 0.521 28.212	0.232 0.532 24.212	**0.217** **0.602** **21.062**
Shapes	0.390 0.493 34.661	0.372 0.512 29.717	0.391 0.472 35.212	0.401 0.517 34.515	0.412 0.492 31.212	0.421 0.461 32.212	0.413 0.512 29.271	0.372 0.571 28.442	0.381 0.635 28.000	0.388 0.562 31.222	0.373 0.591 33.982	**0.354** **0.671** **24.150**

for both the test images, thus showing maximum similarity with the ground truth image.

III.C A BRIEF LOOK INTO THE COMPUTATIONAL TIME FOR THE COMPETING ALGORITHMS

Our algorithm serves to accurately extract the weak edge information from an image and improve edge quality, while regulating noise and maintaining the unique structural characteristics of the image. However, when accuracy is the major bottleneck, computational complexity has to be compromised to a certain extent. Traditional edge detectors do not take perceivable computational time and their performance as complete edge detectors is also compromised as can be observed from their greater deviation from ideality. For example, Roberts cross edge detector performs a 2-D spatial gradient measurement on an image and highlights regions of high spatial frequency, which often correspond to edges. This detector takes very less computational time since only four input pixels need to be mathematically operated upon to determine the value of each output pixel. However, since it uses a very small kernel, it produces very weak responses to genuine edges unless they are in high contrast zones. Sobel detector performs better than Roberts in this aspect as it uses a 3×3 instead of a 2×2 kernel and thus produces higher output values for similar edges than the latter. However, it does not provide significant improvement over the latter in case of weak edge detection. Secondly, the smoothing effect of this operator leads to edges that are several pixels wide which is undesirable. Similarly, for all other traditional edge detectors, performance is compromised despite the unperceivable computational time. Our algorithm involves an optimization strategy and evidently takes larger computational time than the classical edge detectors. However, it is evident from the results provided in Table 7 that our algorithm requires the lowest average computational time per image among all the metaheuristic algorithms and also serves as an accurate edge detection algorithm. It yields better performance by accurately extracting necessary information through an extensive searching of the test image. For the results provided in Table 7, the experiments are carried out on a PC with a second generation core i5 processor running at 2.66 GHZ and having 4 GB RAM. The operating system is Windows 7 home basic and the compiler is MATLAB 7.10.0. The computational time was evaluated after averaging through 25 runs for all of the 9 test images. For the colour images, the computational time was taken as an average of that calculated for each of the individual RGB components and this was added to the final average computational time.

Table 7: Average computational time per image taken by the competing metaheuristic algorithms

Metaheuristic algorithms	Mean computational time in seconds
BFA based edge detector [33]	24.57
Optimal Fuzzy (PSO)	18.23
Optimal Fuzzy (DE)	15.65
Optimal Fuzzy (GSA)	**12.22**

IV. SPECIAL FEATURES OF THE FUZZY APPROACH

Our fuzzy approach provides membership values to all edges, whether strong or weak and hence both strong and weak edges can be demarcated by their distinct membership values. For instance, in the fuzzy edge map of the cameraman test image (Fig. 12(a)), the deeper shades of white correspond to the stronger edges which have higher fuzzy membership values while the weaker

This article has been accepted for publication in a future issue of this journal, but has not been fully edited. Content may change prior to final publication. Citation information: DOI 10.1109/TFUZZ.2013.2286418, IEEE Transactions on Fuzzy Systems

edges have paler shades of white due to their lower membership values. While local adaptive thresholding brings out all the features of an image without differentiating between weak and strong edges as in Fig.12(b), sometimes image segmentation problems depend entirely on human discretion and may require extraction of only the sharper edges or features in the image or simply the weaker edges or minute features. Global thresholding is not applicable on the fuzzy edge map due to spatial variations as is evident from Fig. 12(a). However, if we sort the values in the fuzzy image matrix and set a global threshold depending on the membership value of the *n*-th relatively strong edge, we can suppress the relatively weaker edges or features. Figs. 12(c) - 12(g) have thresholds of 0.45, 0.4, 0.35, 0.3 and 0.25 respectively with the maximum membership value in the fuzzy edge map being 0.4715 and the minimum being 0.1107. Thus, for a selective global threshold of 0.45 as in Fig. 12(c), only a few relatively stronger edge points are extracted and with gradual decrease in the threshold value, it is seen that the finer details and weaker edges (like the grass and the buildings or structures in the background) appear. Evidently Fig.12(e) with a threshold of 0.35 shows the most appropriate edges. Thus, apart from weak edge detection, this method can also be applied to selective demarcation of edges, whether strong or weak.

This feature of our proposed approach can be applied to fat layer detection in meat. As is evident from Fig.13, both our edge detector and the recently developed edge detection scheme [36] perform poorly. Adaptive thresholding was applied on our fuzzy edge map to obtain the image in Fig.13(c) and hence the false edges due to light speckles have appeared just like those in Fig.13(b). However, after applying a selective global threshold of 0.25, the false edges which have a membership value lower than 0.25 get suppressed and thus, we do not need an anisotropic diffusion filter as a pre-processing step.

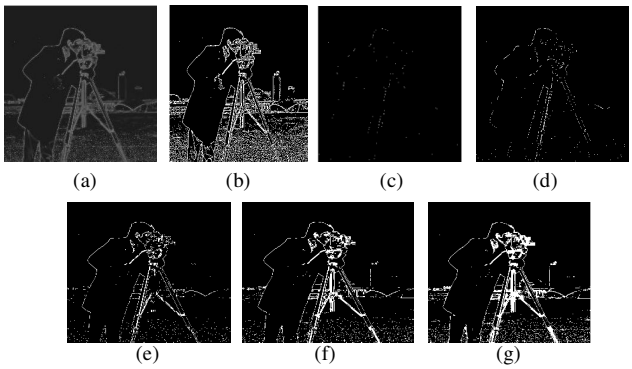

(a) (b) (c) (d)

(e) (f) (g)

Fig.12: (a) Fuzzy edge map (Cameraman) (b) Fuzzy edge map after adaptive thresholding showing all the features. (both weak and strong edges) (c) Edge map (threshold=0.45) (d) Edge map (threshold=0.40) (e) Edge map (threshold=0.35) (f) Edge map (threshold=0.30) (g) Edge map (threshold=0.25)

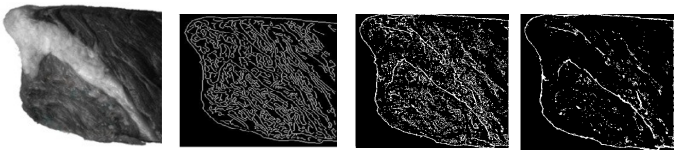

(a) (b) (c) (d)

Fig.13: (a) Meat Image (b) edge map of the algorithm of [36] (c) edge map of proposed approach(d) edge map of the proposed approach with a few suppressed false edges.

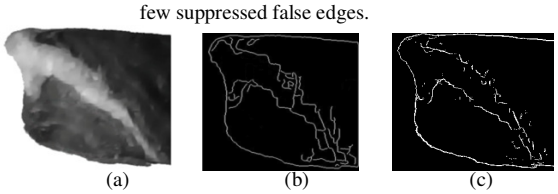

(a) (b) (c)

Fig. 14: (a) Original meat image subject to anisotropic diffusion filter (b) Edge map of the algorithm of [36] (c) edge map using the proposed method showing the most appropriate edges.

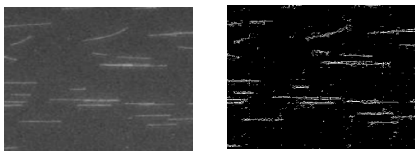

(a) (b)

Fig. 15: (a) Image subject to noise (b) Edge map of noisy image

However, the results would obviously be better after applying the filter as it smoothes out the light speckles in the image as is evident from Fig.14. Since the weak edges have been smoothed out by the filter, both algorithms detect the stronger edges present in the form of the fat layer in the meat. Fig.15 shows the results of our approach for a noisy image. Most of the false edges due to noise have been suppressed by setting a selective global threshold of 0.25. However, some discrete false edge points with membership values above 0.25 are still present. Hence, future research work with this method would be to further improve it for noisy images.

V. CONCLUSIONS

The experimental results show that the proposed optimal fuzzy edge detection algorithm, using GSA, is able to detect weak edges accurately by optimizing the parameters that control the shape of the bell-shaped fuzzy membership function. Bi-level adaptive thresholding [27] binarizes the fuzzy edge maps to yield the spatial domain edge maps for the RGB components in case of a colour image. The main advantage of using this method is that:

a) Our edge detector retains the shape of the image, shows great edge connectivity and has regulated noise content, indicated by the relatively high Pratt's figure of merit and optimal Shannon's Entropy value.
b) Owing to the ability of this edge detector to detect weak edges accurately while still preserving the shape of the object, it can be used in biometric applications like palm print identification, face detection, contour feature extraction, etc.
c) Gravitational Search is a recently developed algorithm. New heuristic algorithms are being devised because the existing optimization techniques cannot

yield optimal solutions for all possible optimization problems. For instance, in our proposed approach, GSA shows better performance than DE and PSO. Comparisons with these algorithms open up new prospects for further research in various other fields.

Future work with the proposed approach would be to extend it for noisy images and images subjected to motion blur. One drawback of this method is that it fails to suppress edges due to substantial amount of noise that distorts the shape of the image. Though the weak edges due to noise can be removed through selective global thresholding as is mentioned in Section V, the method may fail to suppress the stronger edges due to noise if any.

REFERENCES

[1] S. Beucher and F. Meyer, "The morphological approach to segmentation: The Watershed transformation", ER Dougherty Editor, *Mathematical Morphology in Image Processing*, 1993.

[2] J. Kovacevic and M. Vetterli, "Non separable multidimensional perfect reconstruction filter banks and wavelet for R^n", *IEEE Transactions son Information Theory*, Vol.38, Issue 2,pp. 533-555,1992 .

[3] S. Mallat and S. Zhong, "Characterization of signals from multiscale edges*", IEEE Transactions on Pattern Analysis and Machine Intelligence*, Vol.14, Issue 7, pp.710-732.

[4] J. Canny, "A computational approach to edge detection", *IEEE Transactions on Pattern Analysis and Machine Intelligence*, Vol. 8, Issue 1, pp. 679-698,1986.

[5] Y. Yao and H. Ju, "*A* Sub - pixel edge detection method based on Canny operator", Proceedings of 6th*International Conference on Fuzzy Systems and Knowledge Discovery*, Tianjin, pp.97–100, 16-18, Aug. 2009.

[6] S. M. Smith and J. M. Brady, "SUSAN: A new approach to low level image processing", *International Journal of Computer Vision*, Vol. 23, Issue1, pp.45-78, 1987.

[7] C. E. Shannon, "A mathematical theory of communication", *Bell System Technical Journal*, Vol. 27, pp. 379-423, 1948.

[8] I. Bloch, "Fuzzy sets in image processing", *Proceedings of ACM Symposium on Applied Computing*, New York, USA, March 6-8, pp. 175 – 179, 1994.

[9] J. C. Bezdek, R. Chandrasekhar and Y. Attikiouzel, "A geometric approach to edge detection", *IEEE Transactions on Fuzzy Systems*, Vol. 6, Issue l, pp. 52- 75, 1998.

[10] V. Boskovitz and H. Guterman, "An adaptive eneuro-fuzzy system for automatic Image segmentation and edge detection", *IEEE Transactions on Fuzzy Systems*, Vol. 10, Issue 2, pp. 247-261, 2002.

[11] Y. Becerikli and T. M. Karan, "A new fuzzy approach for edge detection", in J. Cabestany, A. Prieto, and D.F. Sandoval (Eds.): *IWANN* 2005, LNCS 3512, pp. 943 – 951, 2005.

[12] M. Pagola, C. Lopez-Molina, J. Fernandez, E. Barrenechea, and H. Bustince, "Interval type-2 fuzzy sets constructed from several membership functions: application to the fuzzy thresholding algorithm", *IEEE Transactions on Fuzzy Systems*, Vol. 21, no. 2, pp. 230-244, Apr. 2013.

[13] E. Barrenechea, H. Bustince, B. De Baets, and C. Lopez-Molina, "Construction of interval-valued fuzzy relations with application to the generation of fuzzy edge images", *IEEE Transactions on Fuzzy Systems*, Vol. 19, No. 5, pp. 819 - 830, Oct. 2011.

[14] F. Russo and G. Ramponi, "Edge extraction by FIRE operators", *Proc. of 3rd IEEE Conference on Fuzzy Systems*, pp. 249 - 253, June, 1994.

[15] F. Russo, "FIRE operators for image processing", *Fuzzy Sets and Systems*, Vol. 103, Issue 2, pp. 265-275, 1999.

[16] L. Jiang, "Image edge detection based on fuzzy weighted morphological filter", *Proceedings of the Eighth International Conference on Machine Learning and Cybernetics*, Baoding, July 12-15, pp. 690 – 693, 2009.

[17] S. E. El-Khamy, I. Ghaleb, N. A. El-Yamany, "Fuzzy edge detection with minimum fuzzy entropy criterion", *Electrotechnical Conference MELECON*, 9-9 May, 2002, Mediterranean, pp. 498-503.

[18] F. Hoeppner, Fuzzy Shell Clustering Algorithms in Image Processing: Fuzzy C-Rectangular and 2-Rectangular Shells, IEEE Trans. on Fuzzy Systems, Vol. 5, No. 4, pp. 599 - 613, 1997.

[19] D. Zhang, B. Zhan, G. Yang, X. Hu, "An improved edge detection algorithm based on image fuzzy enhancement", *Proceedings of 4th IEEE Conference on Industrial Electronics and Applications*, Xi'an, 25-27 May, 2009, pp. 2412 – 2415.

[20] W. Jinbo and Y. Zhouping, "The fast multilevel fuzzy edge detection of blurry image*s*", *IEEE Signal Processing Letters*, 2007, Vol. 14, Issue 5, pp. 344- 347.

[21] X. Chen and Y. Chen, "An improved edge detection in noisy image using fuzzy enhancement", *Proceedings of International Conference on Biomedical Engineering and Computer Science*, Wuhan, April 23-24, 2010, pp.1-4.

[22] E. Rashedi, H. Nezamabadi-pour, and S. Saryazdi, "GSA: a gravitational search algorithm", *Information Sciences*, Vol. 179, No. 13, June 2009, pp. 2232–2248, March 2009.

[23] C. Li and J. Zhou, "Parameters identification of hydraulic turbine governing system using improved gravitational search algorithm", *Energy Convers. Manage.* vol. 52, no. 1, pp. 374–381, 2011.

[24] P. K. Roy, B. Mandal, and K. Bhattacharya, "Gravitational search algorithm based optimal reactive power dispatch for voltage stability enhancement", *Electric Power Components and Systems*, Vol.40, Issue 9, pp. 956 - 976, 2012.

[25] C. Li, J. Zhou, B. Fu, P. Kou, and J. Xiao, "T–S fuzzy model identification with a gravitational search-based hyperplane clustering algorithm", *IEEE Transactions on Fuzzy Systems*, Vol. 20, No. 2, pp. 305 - 317, April 2012.

[26] S. Al Sharhan, "Fuzzy entropy: A brief survey", *The 10th IEEE International Conference on Fuzzy Systems*, pp. 1135 – 1139, 2001.

[27] C. K. Chow and T. Kaneko, "Automatic boundary detection of the left ventride from cineangiograms", *Computers and Biomedical Research*, 1972, Vol. 5, Issue 4, pp.388- 410.

[28] N. Otsu, "A threshold selection method from gray level histogram", *IEEE Transactions on Systems, Man, Cybernetics*, Vol. 9, pp. 62-66, Jan.1979.

[29] S. Das and P.N. Suganthan, "Differential evolution: a survey of the state-of-the-art*", IEEE Transactions on Evolutionary Computing*, Vol. 15, No.1, pp. 4 – 31, February 2011.

[30] J. Kennedy, R. Eberhart, "Particle Swarm Optimization" *Proceedings of IEEE International Conference on Neural Network*, Perth, Australia, IEEE Service Center Piscataway NJ,1995:1942-1948.

[31] K. M. Passino, "Biomimicry of bacterial foraging for distributed optimization and control", *IEEE Control Systems Magazine*, Vol. 22, No. 3, pp. 52 – 67, 2002.

[32] M. Dorigo, V. Maniezzo, and A. Colorni, "Ant system: optimization by a colony of cooperationg agents", *IEEE Transactions on Systems. Man, and Cybernetics-Part B,* 26(1), pp. 29-41, 1996.

[33] O. P. Verma, M. Hanmandlu, P. Kumar, S. Chhabra, and A. Jindal, "A novel bacterial foraging technique for edge detection", *Pattern Recognition Letters,* Vol. 32, Issue 8, pp. 1187–1196, 2011.

[34] J. Cohen, "A coefficient of agreement for nominal scales", *Educational and Psychological Measurement,* 20: 37–46, 1960.

[35] S. B. Wesolkowski, *Color Image Edge Detection and Segmentation: A Comparison of the Vector Angle and the Euclidean Distance Color Similarity Measures*, A thesis presented to the University of Waterloo in fulfilment of the thesis requirement for the degree of Master of Applied Science in Systems Design Engineering Waterloo, Ontario, Canada, 1999.

[36] W. B. Hussein, A. A. Moaty, M. A. Hussein, and T. Becker, "A novel edge detection method with application to the fat content prediction in marbled meat", *Pattern Recognition*, Vol. 44, issue 12, pp. 2959-2970, 2011.

[37] H. Cao, H.-W. Deng, and Y.-P. Wang, "Segmentation of M-FISH images for improved classification of chromosomes with an adaptive fuzzy c-means clustering algorithm", *IEEE Trans. Fuzzy Syst.*, vol. 20, no.1, pp. 1 - 9, Feb. 2012.

This article has been accepted for publication in a future issue of this journal, but has not been fully edited. Content may change prior to final publication. Citation information: DOI 10.1109/TFUZZ.2013.2286418, IEEE Transactions on Fuzzy Systems

Swagatam Das (M'10 – SM'12) is currently serving as an assistant professor at the Electronics and Communication Sciences Unit of Indian Statistical Institute, Kolkata. His research interests include evolutionary computing and pattern recognition. Dr. Das has published one research monograph, one edited volume, and more than 150 research articles in peer-reviewed journals and international conferences. He is the founding co-editor-in-chief of "Swarm and Evolutionary Computation", an international journal from Elsevier. He serves as associate editors of the IEEE Trans. on Systems, Man, and Cybernetics: Systems, IEEE Computational Intelligence Magazine (2014), Neurocomputing, Information Sciences, and Engineering Applications of Artificial Intelligence. He is an editorial board member of Progress in Artificial Intelligence (Springer), Mathematical Problems in Engineering, International Journal of Artificial Intelligence and Soft Computing, and International Journal of Adaptive and Autonomous Communication Systems. He has been associated with the international program committees and organizing committees of several regular international conferences including IEEE WCCI, IEEE SSCI, SEAL, GECCO, and SEMCCO. He has acted as guest editors for special issues in journals like IEEE Transactions on Evolutionary Computation, ACM Transactions on Adaptive and Autonomous Systems, and IEEE Transactions on SMC, Part C. He is the recipient of the 2012 Young Engineer Award from the Indian National Academy of Engineering (INAE).

Mr. Satrajit Mukherjee is currently pursuing his bachelor degree in Electronics and Tele-communication Department of Jadavpur University, Kolkata, India. His research interests include Computer Vision and Pattern Recognition, Fuzzy systems, Control Systems, Machine Learning, Theoretical Optimization. He has published one international journal and one conference article under the supervision of Dr. Swagatam Das.

Mr. Bodhisattwa Prasad Majumder is currently pursuing his bachelor degree in Electronics and Tele-communication Engineering Department of Jadavpur University, Kolkata, India. His research interests include Fuzzy systems, Image processing, Pattern recognition, evolutionary computation, control theory and wireless Censor Networking. He has authored articles in refereed international journals and conference under the guidance of Dr. Swagatam Das.

Mr. Aritran Piplai is currently studying his bachelor degree in Computer Science Engineering Department of Jadavpur University, Kolkata, India. His research interests include Computer vision and pattern recognition, fuzzy systems, evolutionary computing, and control theory. He has published one journal and one conference article to his credit.